

Understanding the Relationship between Sea Ice and Phytoplankton Biomass in the Tallurutiup Imanga

Department of Atmospheric and Oceanic Sciences

McGill University, Montreal

August, 2024

A thesis submitted to McGill University in partial fulfillment of the
requirements of the degree of

Master of Science

©Stéphanie Bergeron

2024-08-05

Abstract

The diminishing extent and thickness of Arctic sea ice have significant implications for phytoplankton productivity and blooms, with potential cascading effects on the entire marine food web and the livelihoods of self-reliant communities. In this study, we identify how the sea ice regime in Tallurutiup Imanga, one of the Arctic's most productive regions, influences phytoplankton growth and phenological changes. To this end, we use satellite observations for sea ice concentration and chlorophyll-a measurements, sea ice arch data, along with a BioGeoChemical model (BiGCIIM) that estimates chlorophyll-a, mixed layer depth, and nutrient concentrations for the period from 2002 to 2022. Results show that the simulated maximum chlorophyll-a levels occur earlier and are positively biased by 20% in Baffin Bay and the North Water when compared with observations. The fact that the simulated maximum chlorophyll-a occurs earlier suggests that satellite observations are missing significant under-ice primary productivity. Observations show that stable ice arches form when weaker northerly winds are present in Nares Strait. The sea ice arch leads to higher primary productivity and lower sea ice concentration. The model, however, is not able to simulate sea ice arches and consequently shows no chlorophyll-a concentration anomalies in the North Water polynya when an arch forms, but captures the observed (wind-related) sea ice concentration anomaly signal in northeast Baffin Bay, with weaker northerly wind leading to higher sea ice concentration (and vice versa). In Jones Sound, the model is not capable of capturing the observed changes in sea ice concentration and chlorophyll-a concentration associated with the presence or absence of ice arches, presumably due to its inability to simulate ice arches, its still too-coarse spatial

resolution, and the fact that it does not consider local sources of nutrients from surrounding glacial melt. Future work includes running the model with high shear resistance in sea ice to capture sea ice arches, running the model at higher resolution, and storing output diagnostics for chlorophyll-a concentration both over open water and under sea ice separately, in order to ease comparison with satellite ocean surface color observations.

Abrégé

La diminution de l'étendue et de l'épaisseur de la glace de mer arctique a des implications significatives pour la productivité phytoplanctonique et leur floraison, avec de potentiels effets en cascade sur l'ensemble de la chaîne alimentaire marine et les communautés auto-suffisantes qui en dépendent. Dans cette étude, nous identifions comment le régime de glace de mer dans le Tallurutiup Imanga, l'une des régions les plus productives de l'Arctique, influence la croissance du phytoplancton ainsi que ses changements phénologiques. À cette fin, nous utilisons des observations satellitaires pour la concentration de glace de mer et des mesures de chlorophylle-a, des données sur les arches de glace, ainsi qu'un modèle BioGéoChimique (BiGCIIM) qui estime la chlorophylle-a, la profondeur de la couche de mélange et les concentrations de nutriments pour la période de 2002 à 2022. Les résultats montrent que les niveaux maximaux de chlorophylle-a simulés se produisent plus tôt et sont positivement biaisés d'environ 20% dans la Baie de Baffin et dans la polynie des eaux du Nord lorsqu'on les compare aux observations. Le fait que la concentration de chlorophyll-a maximum simulée se produise plus tôt suggère que les observations satellitaires ne perçoivent pas une partie significative de la productivité primaire sous la glace. Les observations montrent que les arches de glace stables se forment lorsque les vents du nord sont plus faibles dans le Détroit de Nares. L'arche de glace conduit à une production primaire plus élevée et à une concentration de glace de mer plus faible. Cependant, le modèle ne peut pas simuler les arches de glace et ne montre donc pas d'anomalies de concentration de chlorophylle-a dans la polynie des eaux du Nord lorsque l'arche se forme, mais il capture le signal d'anomalie de concentration

de glace de mer (lié aux vents) dans le nord-est de la Baie de Baffin, avec des vents du nord plus faibles menant à une concentration de glace de mer plus élevée (et vice versa). Dans le Détroit de Jones, le modèle ne peut pas capturer les changements observés de concentration de glace de mer et de chlorophylle-a associés à la présence ou l'absence des arches de glace, vraisemblablement en raison de son incapacité à simuler les arches de glace, de sa résolution spatiale encore trop grossière, et du fait qu'il ne prend pas en compte les sources locales de nutriments provenant de la fonte des glaciers environnants. Les futurs travaux incluent la génération de sorties du modèle avec une résistance au cisaillement plus élevée de la glace de mer pour capturer les arches de glace, une résolution plus fine, et le stockage des sorties diagnostiques pour la concentration de chlorophylle-a à la fois en eau libre et sous la glace séparément, afin de faciliter la comparaison avec les observations satellitaires de la couleur de la surface de l'océan.

Acknowledgements

First and foremost, I would like to thank my family, who were always the first to celebrate my joys. More specifically, to my father, *Éric*, who believed in me even when I doubted myself, and who always had a kind word to ease my hectic days. To my mother, *Josée*, whose strength of character and eternal optimism have been most comforting. To my brother, *Francis*, who always knew how to make me laugh and distract me during my lows. And to my ever-supportive partner, *Antoine*, thank you for keeping me on track and reminding me of my goals.

Through the rough times of this master's journey, I discovered how challenges bring out the best in friendships. As Marcus Tullius Cicero once said, "Friendship improves happiness and abates misery, by the doubling of our joy and the dividing of our grief." Therefore, I would like to thank all the dear friends I have made along my academic career. Among others, my office mate and great friend, *Madeleine Fol*, I thank you for your kind ear, the crispy gossip, and for never doubting me during this adventure.

Lastly, I am grateful to my supervisors, *Bruno Tremblay* and *Simon Bélanger*, without whom this project would never have seen the light of day. Your immense knowledge, insightful comments, and profound patience were incommensurably helpful.

Table of Contents

Abstract	i
Abrégé	iv
Acknowledgements	v
List of Figures	x
List of Tables	xi
1 Introduction	1
2 Data and Methods	4
1 Study Area	4
2 Data	4
2.1 Chlorophyll-a Concentration ([Chl-a])	4
2.2 Sea Ice Concentration (SIC)	6
2.3 Sea Ice Arches	7
2.4 Sea Level Pressure (SLP)	7
2.5 BiGCIIM Model	7
3 Data processing and analysis	8
3.1 Sea Ice Concentration	8
3.2 Day of Sea Ice Retreat (DSIR) and Day of Partial Ice Cover (DPIC) . .	9
3.3 Sea ice Arches	9
3.4 OC-CCI Chlorophyll-a concentrations	9
3.5 BiGCIIM outputs	10

3	Results	11
1	Chlorophyll-a Climatology	11
2	Sea Ice Arches vs productivity	13
2.1	Nares Strait Arch (NSA)	13
2.2	Jones Sound Arch (JSA)	15
4	Conclusions	25
5	Data Availability Statement	28
A	Appendices	29
1	Appendix A	29

List of Figures

2.1	Map of the Tallurutiup Imanga region as defined by Parks Canada (shaded green) with key geographical, polynya and recurrent sea ice arches locations in Nares Strait (NSA), Jones Sound (JSA) and Lancaster Sound (LCS). JS and LS stands for Jones and Lancaster Sounds.	5
3.1	Observed (OC-CCI) climatology (a, c and g), sea ice concentration CDR climatology for the 2002-2022 period (e) and simulated BiGCIIM chlorophyll-a (b, d, and h) and sea ice concentration climatology (f) for the May 1 st to September 30 th , 2002-2021 period. Average maximum surface chlorophyll-a concentration (on a log scale) (a, b), average Julian day of the maximum surface chlorophyll-a concentration (c, d), average sea ice concentration on day of maximum chlorophyll-a concentration (e, f) and average Julian day transition between ice-covered area and open water (SIC = 15%) (g, h). . . .	17
3.2	Standard deviation for average maximum (a,b) and Julian day (c,d) surface chlorophyll-a concentration, average sea ice concentration on day of maximum chlorophyll-a concentration (e, f) and and average Julian day transition between ice covered area and open water (SIC = 15%) (g,h). From May 1st to September 30th for OC-CCI climatology (2002-2022) (a, c and g), sea ice concentration CDR climatology (2002-2022) (e) and BiGCIIM climatology (2002-2021) (b, d, f and h).	18

3.3 Difference between the average day of chlorophyll-a maximum and the day of partial ice cover (DPIC, i.e., the first Julian Day of $SIC \leq 85\%$) in BiGCIIM (a), and the climatological occurrence (%) when the average chlorophyll-a maximum occurs before the start of partial ice cover from 2002 to 2021 (b). 19

3.4 Difference in sea ice concentration in May (top panel) and chlorophyll-a concentrations from May 1st to September 30th (bottom panel) between the years with and without (2007, 2009, 2010, 2017, 2019) the Nares Strait Arch, for the observations from 2002 to 2022 (left column) and BiGCIIM from 2002 to 2021 (right column). Black contours indicate regions with a high grid density of data significant at the 95% level, smoothed using kernel density estimation (left column). 20

3.5 Difference in nitrate concentrations (a), ammonium concentrations (b) and mixed layer depth (c) from BiGCIIM between years with and without (2007, 2009, 2010, 2017, 2019, 2022) the Nares Strait Arch (NSA) from May 1st to September 30th for the period from 2002 to 2021. Black dots show grid cell with 95% significant difference. 21

3.6 Difference in the composite of sea level pressure (Pa) from MERRA-2 between years with and without (2007, 2009, 2010, 2017, 2019, 2022) the Nares Strait Arch (NSA) for the month of March, April and May from 2002 to 2022. 22

3.7 Difference in sea ice concentration in May (top panel) and chlorophyll-a concentrations from June 1st to September 30th (bottom panel) between the years with and without (2003, 2004, 2006, 2009, 2022) the Jones Sound Arches (JSA), for the observations from 2002 to 2022 (left column) and BiGCIIM from 2002 to 2021 (right column). Black contours indicate regions with a high grid density of data significant at the 95% level, smoothed using kernel density estimation (left column). 23

3.8	Difference in composite of sea level pressure (Pa) from MERRA-2 between years with and without (2003, 2004, 2006, 2009, 2022) the Jones Sound Arch (JSA) for the months of March, Avril and May from 2002 to 2022.	24
A1	Average maximum chlorophyll-a concentrations variation coefficient (%) for the productive season, from May 1 st to September 30 th , for OC-CCI observations from 2002 to 2022 (a) and BiGCIIM from 2002 to 2021 (b). . . .	29
A2	Temporal series of years with (green square) and without (red triangle) sea ice arch in the Nares Strait, Jones Sound and Lancaster Sound for May from 2002 to 2022.	30
A3	Difference between the average day of chlorophyll-a maximum and the day of partial ice cover (DPIC, i.e., the first Julian Day when SIC specified thresholds) in BiGCIIM (left column), and the occurrence (%) when the average chlorophyll-a maximum occurs before partial ice cover at different SIC thresholds (50%, 75%, 80%, 90%, and 95%) from 2002 to 2021 (right column).	31

List of Tables

2.1 Satellites used to derive chlorophyll-a concentration in OC-CCI (version 6) from 2002 to 2022.	6
---	---

Chapter 1

Introduction

The Arctic sea ice has witnessed a significant reduction of 22% in sea-ice extent over the last four decades and lost more than 50% of its multi-year ice from 1999 to 2017, now covering less than one-third of the Arctic Ocean (35; 77). In Baffin Bay, sea-ice thickness has declined significantly, at a peak rate of 15 cm per decade in April from 1996 to 2020 (23). As the older ice disappears, the sea-ice cover is increasingly composed of thinner, weaker, less-reflective seasonal ice [albedo of bare multi-year and first-year sea ice are ~ 0.62 and ~ 0.37 , respectively] with an increased melt pond area, all acting as positive feedback on the sea loss (21; 51; 56).

Ocean biological productivity is profoundly impacted by these ongoing changes in ice cover, which control light availability and surface ocean vertical mixing (1). Generally, an earlier sea ice retreat allows for an earlier onset of phytoplankton productivity and an extended productive season, since it is often light-limited (4; 6; 9). Satellite observations show an increase in the Arctic Ocean's net primary productivity over the last decades, with the recent rise being attributed to an increase in phytoplankton biomass (39). These trends in primary production, however, are not spatially homogeneous (9; 39) and depend on local geographical and oceanic conditions.

The northern Baffin Bay, one of the most productive arctic marine systems (33; 72), is among the regions where the trend in primary production remains unclear (9; 39). On the one hand, satellite and *in situ* observations revealed a 65% decline in net primary productivity from 1997 to 2011, suggesting that nutrient-limitation can also be significant in northern Baffin Bay (9; 10; 12). Surface water freshening due to increasing sea ice melt strengthens the surface stratification, leading to less vertical mixing and reduced upward nutrient flux (10). On the other hand, satellite observations, (48) reported that the productivity of the North Water (NOW) polynya has remained high despite the changing ice cover dynamic. Regardless, as surface water warms, stratification increases, and a prevalence of smaller organisms can be expected (40; 73). Additionally, changes in phytoplankton phenology (2; 8), as observed in the northern Baffin Bay (43), can potentially lead to a desynchronization between phytoplankton bloom and grazers appearance, ultimately disturbing upper trophic levels (53). Finally, even before the complete retreat of the ice pack, changes in sea ice regime allow for more photosynthetically active radiation to penetrate the snow and ice cover, promoting under-ice blooms, sometimes up to 50% of the annual primary production in the Canadian Archipelago (3; 49).

A prolonged period of open water conditions results in continuous sea ice formation, salt rejection, and the deepening of the mixed layer during winter, followed by an abundance of nutrients in spring associated with wind-driven mixing and convection (58). As a result, these large ice-free areas provide a sustainable environment for diverse Arctic species, including narwhal, beluga, walrus, and polar bear (58). The recent loss of multi-year ice, however, has resulted in a thinner and weaker first-year sea-ice cover, decreasing the stability of ice arches and easing the export of sea ice through straits (25). Notably, the number of days with a blockage in the Nares Strait decreased by 2.1 days per year from 1979 to 2019 (75), hence, threatening the stability of the North Open Water (NOW) and Jones Sound (JSP) polynya (25; 48). Further examination of the biological response to the changing ice cover conditions in the Canadian Arctic Archipelago remains to be estab-

lished.

The study of primary productivity at high latitudes is challenging due to sparse *in situ* observations and the limitations of ocean color satellites in the presence of sea ice, cloud cover and low sun angle (30). This motivated the development of holistic biogeochemical models for a simplified representation of ocean biological cycles. This first such model widely used in the community is the Biogeochemical, Light, Iron, Nutrient, and Gases (BLING) model, a simplified model coupled with the Nucleus for European Modelling of the Ocean (version 3.6, NEMO3.6) and Louvain-la-Neuve sea Ice Model (version 2, LIM2) ice-ocean model (42; 74). Given that BLING was developed to study phosphate and iron limitation on physiological processes affecting phytoplankton growth globally but that Arctic and sub-Arctic regions are, in fact, nitrogen-limited (38; 70; 71), we use instead the more complex BioGeoChemical Ice Incorporated Model (BiGCIIM) coupled to the same physical ocean and sea ice model framework as BLING (17).

In the following, we both observed and simulated chlorophyll-a concentrations from the newly developed biogeochemical model BiGCIIM, and to assess the affects of sea ice changes on primary productivity within the study area. Given the relatively short time series of satellite observation we use composites of primary productivity between years with and without the Nares Strait (NSA) and Jones Sound (JSA) arches.

Chapter 2

Data and Methods

1 Study Area

In this paper, we focus on the Tallurutiup Imanga (NMCA) (Figure 2.1), a protected region of 108 000 km² located within the northeast Nunavut Territory (55). The coastal land and seascape of Tallurutiup Imanga are protected by the Canada National Marine Conservation Areas Act with the goal of preserving a critical habitat for various large mammals, such as polar bears, narwhal, walrus and beluga whales on which nearby Inuit communities rely on (52). This region is characterized by thick multi-year sea ice, with a highly productive polynya downwind with sea-ice arches forming a bridge between irregular features of the coastline preventing downstream sea-ice drift and creating large and long-lasting open water area (48). Example of these include the Nares Strait (NSA) and Jones Sound (JSA) arches, and North Water and the Jones Sound polynya (36; 58; 75).

2 Data

2.1 Chlorophyll-a Concentration ([Chl-a])

We use the European Space Agency (ESA) Ocean Colour Climate Change Initiative (OC-CCI) ocean color dataset (version 6) from 2002 to 2022 stored on the polar stereographic

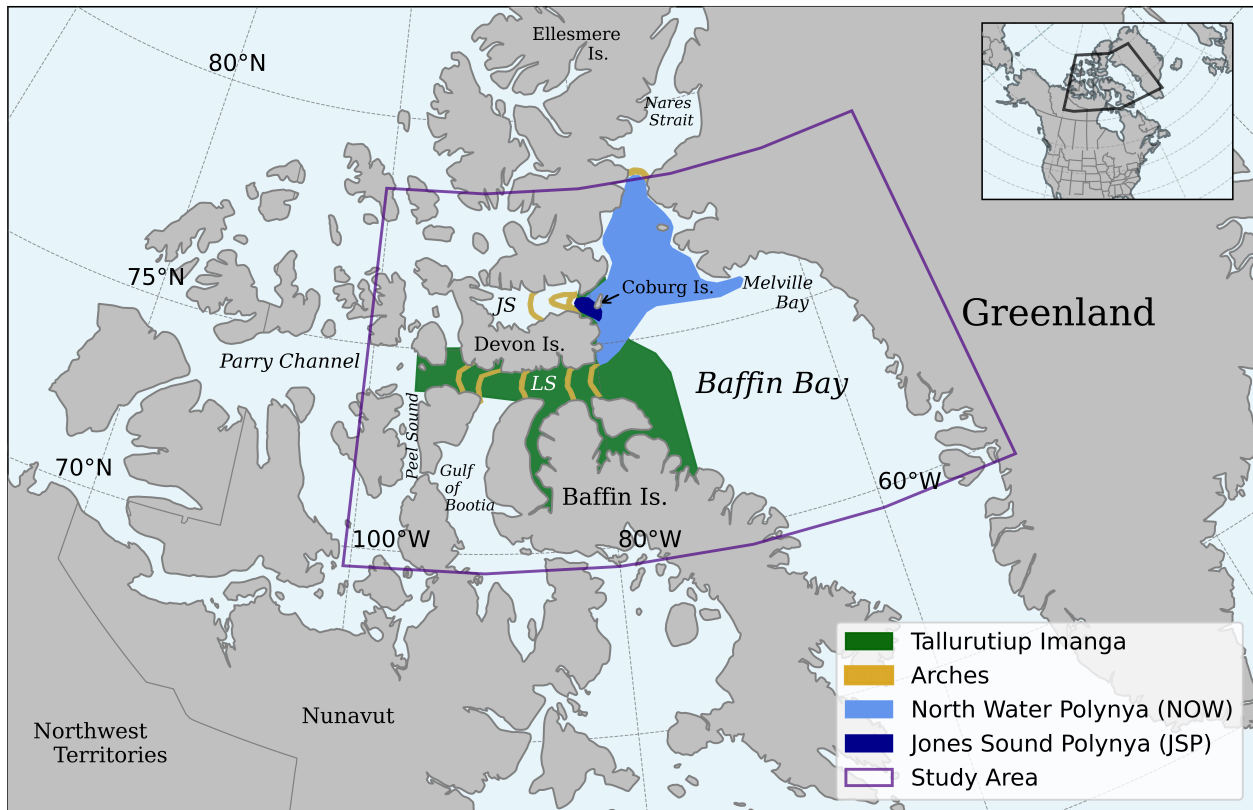


Figure 2.1: Map of the Tallurutiup Imanga region as defined by Parks Canada (shaded green) with key geographical, polynya and recurrent sea ice arches locations in Nares Strait (NSA), Jones Sound (JSA) and Lancaster Sound (LCS). JS and LS stands for Jones and Lancaster Sounds.

projection (ESPG 3411) (62). The dataset is derived from merged ocean colour observations from the Sea-Viewing Field-of-view Sensor (SeaWiFS), the Medium Resolution Imaging Spectrometer (MERIS), the Moderate Resolution Imaging Spectroradiometer-Aqua (MODIS-Aqua), the Visible Infrared Imaging Radiometer Suite (VIIRS), and the Ocean and Land Colour Instrument onboard Sentinel 3A and 3B (OLCI 3AB) (Table 2.1, (60)). The use of multiple sensors significantly reduced the number of missing data days while improving spatial coverage (34). Briefly, the OC-CCI reflectance data obtained from the satellite sensors were band-shifted to match the SeaWiFS wavebands, merged and processed using the in-water bio-optical algorithm to generate daily chlorophyll-a concentration maps at 4 km nominal resolution (60). The MERIS and SeaWiFS, MODIS-Aqua

Table 2.1: Satellites used to derive chlorophyll-a concentration in OC-CCI (version 6) from 2002 to 2022.

Satellite	Active Period
SeaWiFS	Sep 1997 - Dec 2010
MERIS	Mar 2002 - May 2012
MODIS-Aqua	May 2002 - Jun 2020
VIIRS	Oct 2011 - Jun 2020
OLCI 3AB	Feb 2016 - Dec 2022

and VIIRS data are corrected using the POLYMER atmospheric correction algorithm and the NASA’s `l2gen` processor, respectively. Chlorophyll-a, a pigment present in all primary producers, influences the backscattered signal captured by satellites and serves as a proxy for phytoplankton biomass (28).

2.2 Sea Ice Concentration (SIC)

We use the daily National Oceanic and Atmospheric Administration (NOAA) and National Snow and Ice Data Center (NSIDC) sea ice concentration (SIC) Climate Data Record (CDR) (version 4) for the period from 1979 to present. The passive microwave brightness temperature data are from the Defense Meteorological Satellite Program’s Special Sensor Microwave Imager (SSM/I) and Sounder (SSM/IS), and the Nimbus-7 Scanning Multichannel Microwave Radiometer (SMMR). The CDR algorithm combines two SIC products from the NASA Team (NT) and the NASA Bootstrap (BT) algorithms, (15; 16) capitalizing on the strengths of each individual dataset to minimize errors (46). The CDR is stored on the polar stereographic projection (ESPG 3411) with a nominal resolution of 25×25 km (45). Errors in the CDR sea ice concentration ranges between 5 and 10% during winter and can rise up to 30 to 40% in summer due varying melt ponds coverage, leads opening and ice edges (31).

2.3 Sea Ice Arches

We used the weekly sea ice arches dataset compiled from visual analysis of Ice Charts from the Canadian Ice Service (CIS) and Danish Meteorological Institute (DMI) for the period 1968 to 2023 (13; 64). The use of both CIS and DMI ice charts leads to a reduced error and enhanced temporal coverage and was preferred to the use of sea ice concentration data based on insufficient resolution (36). A polynya in the NOW is identified if sea ice concentration is at least 90% upstream of a concave line, between Ellesmere Island and Greenland, located at 78.6°N , 74°W in the Nares Strait. Similarly, a polynya in the Jones Sound is identified if an ice arch is present between Devon and Ellesmere islands located at 75.5°N and from 82° to 86°W (Figure 2.1).

2.4 Sea Level Pressure (SLP)

We used the sea level pressure data from the NASA Modern-Era Retrospective Analysis for Research and Applications, Version 2 (MERRA-2) reanalysis dataset, from March to May from 2002 to 2022(24). MERRA-2 ingests a wide variety of satellite and conventional observations, summarized in (22). Data are assimilated into the Goddard Earth Observing System Version 5 (GEOS-5) atmospheric model according to a 3D variational scheme, with updates 6 hourly (22). Then GEOS-5 uses cubed-sphere geometry at an approximate horizontal resolution of $0.5^{\circ} \times 0.625^{\circ}$, and 72 hybrid-eta levels from the surface to 0.01 hPa. Detailed information on model physics and the assimilation algorithm are available in (59).

2.5 BiGCIIM Model

We use the BiGCIIM model coupled to the NEMOv3.6 ocean and LIM2 ice models and (42; 74). The primitive equation ocean physics model allows for a $1/4$ degree nominal horizontal resolution (ANHA4) and better resolution of small-scale ocean processes, which can be biologically relevant (14; 50). The model was run from January 1st, 2002 to De-

ember 31st, 2021 on the tripolar Arctic, Northern Hemisphere Atlantic grid with 50 vertical levels from the surface to ~ 5500 m with increasing thickness from 1.05 to 453.13 m thickness at the lowest level, 16 minutes time-step and 5-day mean output diagnostic. This configuration has two open boundaries, one close to Bering Strait and the other at 20°S across the Atlantic Ocean (26). The ocean model is hydrostatic and eddy-permitting (14; 50). LIM2 has three-layers (one snow and two ice layers of equal thickness), is based on the modified elastic-viscous-plastic (mEVP) ice rheology and considers light attenuation through snow and ice (26; 32). BiGCIIM is a Nutrient, Phytoplankton, Zooplankton, and Detritus (NPZD) biogeochemical model that includes dissolved organic nitrogen, nitrate and ammonium, dissolved inorganic nitrogen, particulate organic matter and has two phytoplankton and zooplankton groups in the ocean with ice algae, fauna and nitrate in the ice. BiGCIIM uses a nutrient fraction limitation between nitrate and ammonium for both in sea ice (sympagic) and ocean (pelagic) biology (17). Improvements from previous biogeochemical models include the integration and upgrade of sea-ice biogeochemistry (sympagic, (65)), computation of solar radiation through ocean and ice within a grid cell to represent phytoplankton growth in partial ice-covered areas more accurately (41) and implementation of nitrification and remineralization rates to ensure closed-loop biogeochemistry (17).

3 Data processing and analysis

3.1 Sea Ice Concentration

The sea ice concentrations are interpolated onto the 4 km resolution Chlorophyll-a dataset using bilinear interpolation. The choice of bilinear interpolation is based on its balance between efficiency and the risk of altering extreme values (57).

3.2 Day of Sea Ice Retreat (DSIR) and Day of Partial Ice Cover (DPIC)

We define the day of sea ice retreat (DSIR) as the first occurrence when sea ice concentration drops below 15%, in a given year for each grid cells (19; 66; 67). The day of partial ice cover (DPIC) is defined as the first occurrence in a given year when the sea ice concentration (SIC) drops below thresholds of 50, 75, 80, 85, 90, or 95 % for each grid cell.

3.3 Sea ice Arches

We consider an ice arch present if it is present in at least one week in May in the joint weekly CIS-DIM sea ice arch dataset (48). The month of May is chosen because it is the beginning of the productive season and the moment when the ice is thickest and can best sustain a stable ice arch. The area of influence of the Nares Strait (NSA) and Jones Sound (JSA) arches are defined as the North Open Water (NOW) (72.5° to 78.5° N and 68° to 79° W) and the Jones Sound (JSP) polynya (75° to 76.6° N and 81° to 91° W) (figure 2.1).

3.4 OC-CCI Chlorophyll-a concentrations

Satellite observations of ocean colors may contain outliers that inaccurately represent biomass productivity. To eliminate these values, the satellite dataset has been pre-processed using a median filter with a 7-day window over each grid cell for every year from 2002 to 2022, naturally eliminating outliers that surpass the $100 \text{ mg}/\text{m}^3$ threshold. We define the productive months for each polynya only for satellite observations, when a threshold of $0.5 \text{ mg}/\text{m}^3$, in each grid cell in the daily chlorophyll-a concentration data spanning from 2002 to 2022. If the majority of grid cells within the area of influence, defined in the previous section, surpassed this threshold, the corresponding month was classified as productive for that polynya. The productive season for the NSA and JSA spans from May to September and from June to September, respectively.

3.5 BiGCIIM outputs

First, we concatenated along the time axis the daily model output files using the Climate Data Operators (CDO) (63). We use chlorophyll-a concentrations from diatoms and flagellates (in mg/m^3), with total phytoplankton biomass comprising the sum of contributions from diatoms and flagellates. Following (61), we define the simulated surface [chl-a] that would be seen by satellites as the average of the top 10 meters of the water column. Chlorophyll-a concentrations exceeding $100 mg/m^3$ are considered non-valid values, similar to treatment of satellite observations. Nitrate and ammonium concentrations in the top 10 meters (in $mmol/m^3$), along with mixed layer depth (in m), already computed by the model using the $\Delta\sigma$ computational method, were also used. To focus on the productive season, the datasets are temporally sliced from May 1st to September 30th from 2002 to 2021 using Python and the NumPy library.

Chapter 3

Results

1 Chlorophyll-a Climatology

Since BiGCIIM primary productivity data are not limited by sea ice concentration, comparing these data with satellite observations in figure 3.1 helps determine whether productivity intensity and timing is limited by light or nutrients. Satellite observations show a similar spatial pattern for the maximum chlorophyll-a concentration [chl-a], sea ice concentration (SIC) at maximum [chl-a], day of maximum biomass, and day of sea ice retreat, with larger and earlier [chl-a] maxima along the west coast of Greenland, the North Water polynya, the Tallurutiup Imanga region and Jones Sounds (OC-CCI; Figure 3.1, left panels). One key exception includes the sea ice concentrations and day of sea ice retreat that extend farther south along Baffin Island. Simulation results from BiGCIIM (Figure 3.1, right panels) show a similar spatial pattern, albeit with much-reduced contrast between highly productive and less productive areas and higher overall surface concentration by about 20%, much earlier day of maximum [chl-a], significantly later day of sea ice retreat and much higher SIC when the maximum [chl-a] occur. The overestimate in [chl-a] is a common issue in biogeochemical models (7; 18). In contrast with observations, the east coast of Baffin Island, Gulf of Bootia, Jones and Peel Sounds all show higher maximum [chl-a], earlier day of maximum [chl-a] and DSIR. The discrepancy in sea ice retreat tim-

ing between observations and models may be due to LIM2's inability to parameterize landfast ice (27) or, as suggested by (44), LIM2's uniform ice thickness distribution, which leads to underestimating thin sea ice concentration in early spring.

Despite differences in the average magnitude over the entire study area (1.5 in observation vs. $3\text{mg}/\text{m}^3$ in the model), both model and observations indicate that [chl-a] is most variable in the NOW region (Figure 3.2 a, b). Note that the model shows greater variability even normalized with respect to average [chl-a], where coefficient of variation ranges from 20 to 40%, compared to 10 to 30% in the observations (Figure A1, Appendix A). While the observed variability in the day of sea ice retreat is low in Baffin Bay, the day of maximum [chl-a] and SIC at maximum [chl-a] show much larger variability, suggesting either that productivity in the Tallurutiup Imanga region is mainly light-limited or, as suggested above, that the 15% threshold used to determine the timing of sea ice retreat and phytoplankton productivity in observations is not applicable for the model. Along the West Greenland coast, the day of maximum [chl-a] and day of sea ice retreat coincide (Figure 3.1), while variability in maximum [chl-a] is low [$\leq 2\text{mg}/\text{m}^3$], indicating that the ocean is light-limited rather than nutrient-limited. In the model, inter-annual variability is low across all four fields, except for the NOW region where variability in maximum [chl-a] and SIC at maximum [chl-a] is larger, suggesting light limitation is also present in the model (Figure 3.2, right panels).

In sharp contrast with observations, simulated SIC at maximum [chl-a] is typically $>90\%$, except for the North Water where lower sea ice concentrations are present when [chl-a] peaks (Figures 3.1, e). Satellite observations indicated that the maximum [chl-a] occurs at much lower SIC, between 10 and 50%, which is expected since ocean color sensors are limited to open water only. Nevertheless, these differences in SIC at the peak of phytoplankton concentration suggest that under-ice productivity is significant in models, something that cannot be assessed using satellite observations but generally agrees

with *in situ* measurements (3; 47; 54). The day of maximum [chl-a] in the model coincides with the timing when SIC is still present for most of Baffin Bay (with high frequency of occurrence) in support of this hypothesis. To illustrate this feature, we plot the difference between the day of the peak [chl-a] and the day when SIC drops below an arbitrary threshold of 85% (Figure 3.3, a). Negative values indicate chlorophyll-a peaks when the ice cover is almost complete, while positive values indicate chlorophyll-a peaks in reduced ice cover. It should be noted that the SIC threshold used to determine the occurrence of an under-ice peak is important (see Appendix A, Figure A3). With a threshold of 95%, virtually no under-ice bloom was generated by the model. At 90%, less than half of Baffin Bay shows an under-ice [chl-a] maximum, and the occurrence is less than 50%. The tipping point in the model for reaching peak biomass is the SIC threshold is raised from 90% to 85% (Appendix A). In the NOW, eastern Jones Sound and most of the coastal zones of Baffin Bay, phytoplankton concentrations peak after SIC drop below 85% (≥ 40 days, Figure A3, a). In the central Baffin Bay and most of the CAA, under-ice maxima frequency is $\geq 70\%$ if the time (Figure A3, b). In the central Baffin Bay, this under-ice maximum [chl-a] pattern matches the latest and lowest [chl-a] maxima obtained from satellite observations, indicating the inability to capture the true maximum from remote sensing in these areas.

2 Sea Ice Arches vs productivity

2.1 Nares Strait Arch (NSA)

Stable sea ice arches in Nares Strait form when weaker northerly winds are present in northern Baffin Bay (48). For instance, for years without the NSA, the median North Atlantic Oscillation index (NAO) for the three months preceding May is positive (NAO = 1.6), with below-normal surface sea-level pressure in high latitudes, stronger northerly winds and colder air over the Baffin Bay (29; 37; 68). This is clearly seen where lower

(negative values) SIC in Smith Sound and along the east coast of Ellesmere Island and more (positive values) sea ice in northern Baffin Bay downwind of the Greenland coast because of stronger coastal divergence in the presence of NSA (Figure 3.4, top row). The dipole in SIC can also be seen in the chlorophyll-a with higher (positive values) concentrations along the coast of Ellesmere Island when an arch is present (Figure 3.4, bottom row). This higher [chl-a] along Ellesmere Island in the presence of the NSA, may be due to increased vertical mixing and high nutrient concentration associated with new ice formation and salt rejection that dominates over reduced mixing associated with weaker winds. An alternative explanation could be the southern advection of clear oligotrophic and low-salinity Arctic waters with a shallow mixed layer in the absence of NSA. The difference in mixed layer depth (MLD) from the model does not fully support the latter, as thinner mixed layers (negative values) are simulated in a small area south of Smith Sound along Ellesmere Island when the NSA is present (Figure 3.5c).

In the model, only the shadowing effect of the Greenland coast is visible, and no ice arch forms, a common issue with sea ice models that are run with default parameter for shear strength (20), resulting to a positive [chl-a] anomaly, in the absence of arch, along the Ellesmere Island (Figure 3.4, d). In this case, there is a weaker signal in SIC compared to observation, and surface wind mixing is the only factor affecting vertical mixing. This is clearly seen in the western Baffin Bay with lower [chl-a] and lower NO_3 and NH_4 concentrations used by diatoms and flagellates for primary productivity, when an ice arch is present or when winds are weaker (Figure 3.5, a and b). In the model, the MLD of the Baffin Bay was deeper when the NSA is present (NAO negative and weaker northerly winds), with one key exception in the NOW along Ellesmere and east of Devon Islands (Figure 3.5, c). Negative NAO is associated with weaker northerly winds reducing the strength of the Baffin Island Current and West Greenland Current, bringing cold low-salinity Arctic outflows southward and warmer, saltier Atlantic Waters northward, and reducing the strength of Ekman upwelling at the center of Gyre, leading to a deeper

mixed-layer depth (Figure 3.6). Interestingly, the extension of the nitrate signal along Baffin Bay's east coast and at the entrance of the Lancaster Sound appears to originate from the Parry Channel instead. The anomaly pattern of NO_3 in the model roughly mimics the [chl-a] pattern observed in the satellite data, with higher biomass in areas showing depleted NO_3 (Figure 3.4, c versus Figure 3.5, a). In the Baffin Bay, primary productivity is dominated by diatoms and *Phaeocystis* ssp, known to be mainly limited by nitrate and silicate concentrations (69), contrasting with lower concentrations observed on the eastern side. This pattern is presumably linked to deeper mixed layer depths, which facilitate the upward transport of nutrients from deeper water masses where nutrient inventories are more abundant in Baffin Bay than other basins (71).

2.2 Jones Sound Arch (JSA)

We see lower SICs west of Coburg Island when a sea ice arch forms in the Jones Sound and a similar but weaker signal in Lancaster Sound, where arches form simultaneously 60% of the time (see Figures A2 and 3.7, a). The local SIC impact is in contrast with previous studies stating that the Jones Sound ice arches influence sea ice conditions southward, east of Devon Island and at the mouth of Lancaster Sound (76). The weaker signal in Lancaster Sound coincide with the more frequent penultimate arch location (from west to east, see Figure 2.1). The coincident higher SIC in northern Baffin suggests that anomalous westerly winds are responsible for the formation of a sea ice arch in Jones Sound (see also composite of late winter SLP, Figure 3.8). The signal in [chl-a] does not coincide with the SIC signal and, instead, shows a weak signal of highs and lows from west to east roughly aligned with the locations of sea ice arches observed in both sounds (see Figure 2.1). Finally, a relatively strong positive anomaly in [chl-a] in the western part of Jones Sound presumably due to local source of nutrients as opposed to a sea ice arch downstream (Figure 3.7, c).

The model simulates a positive SIC anomaly west of Coburg Island for years when an arch is present in accord with observations but simulates a negative sea ice anomaly in northern Baffin Bay in contrast with observations and the fact that anomalous westerlies are present in late winter (see Figure 3.8). The simulated positive anomaly in [chl-a] in the west part of Nares Strait and along the Ellesmere, Devon and Baffin islands is in contrast with satellite observations, particularly in Lancaster Sound and downstream along the coast of Baffin Island. The poor representation of SIC and [chl-a] anomalies are attributed to the poor spatial resolution and the absence of simulated sea ice arches. In addition, phytoplankton concentration in Jones Sound may be more strongly influenced by local inputs of nutrients from glacier runoff and subsequent mixing processes at marine-terminated glaciers that are not included in the model (11).

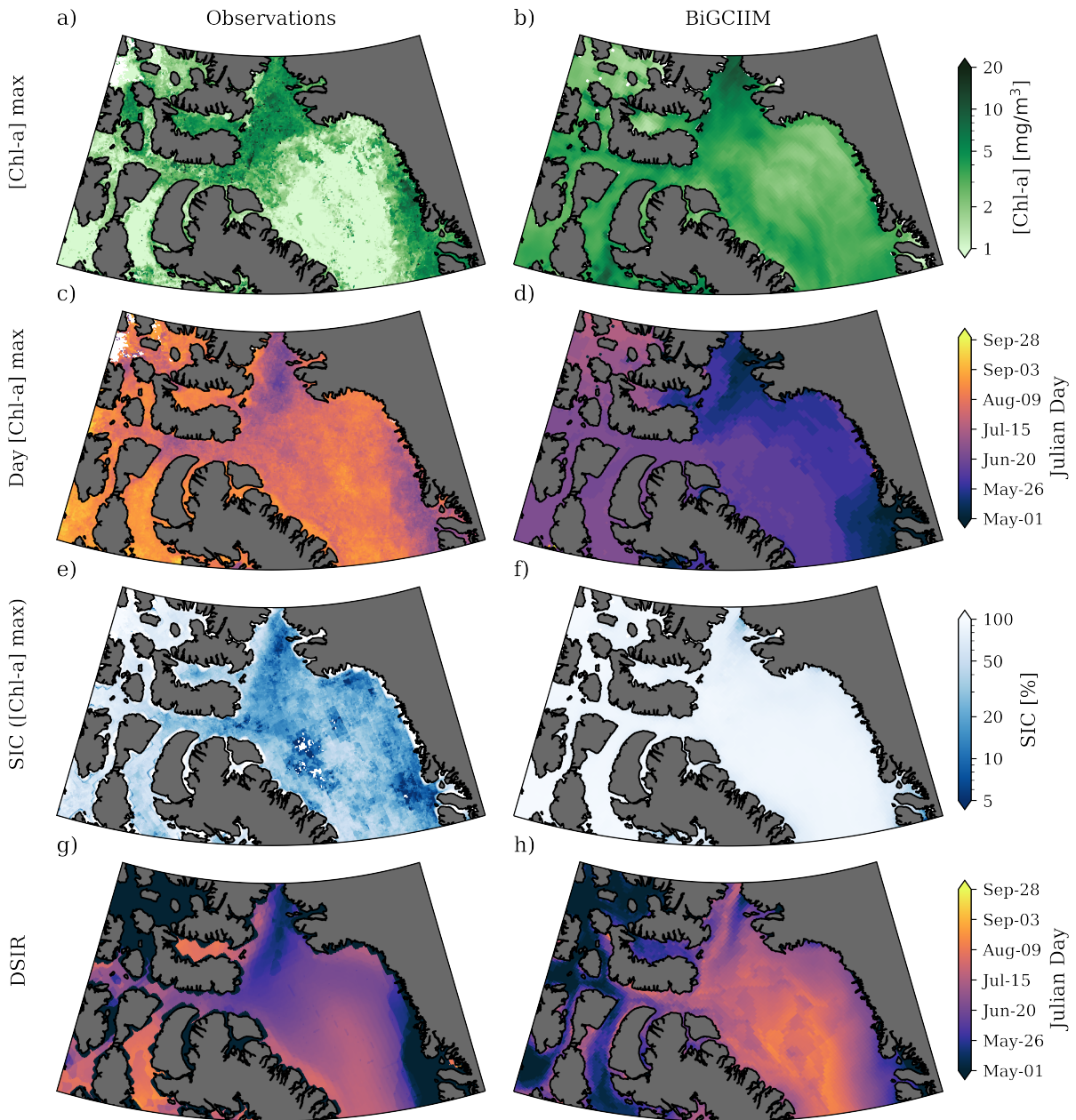


Figure 3.1: Observed (OC-CCI) climatology (a, c and g), sea ice concentration CDR climatology for the 2002-2022 period (e) and simulated BiGCIIM chlorophyll-a (b, d, and h) and sea ice concentration climatology (f) for the May 1st to September 30th, 2002-2021 period. Average maximum surface chlorophyll-a concentration (on a log scale) (a, b), average Julian day of the maximum surface chlorophyll-a concentration (c, d), average sea ice concentration on day of maximum chlorophyll-a concentration (e, f) and average Julian day transition between ice-covered area and open water (SIC = 15%) (g, h).

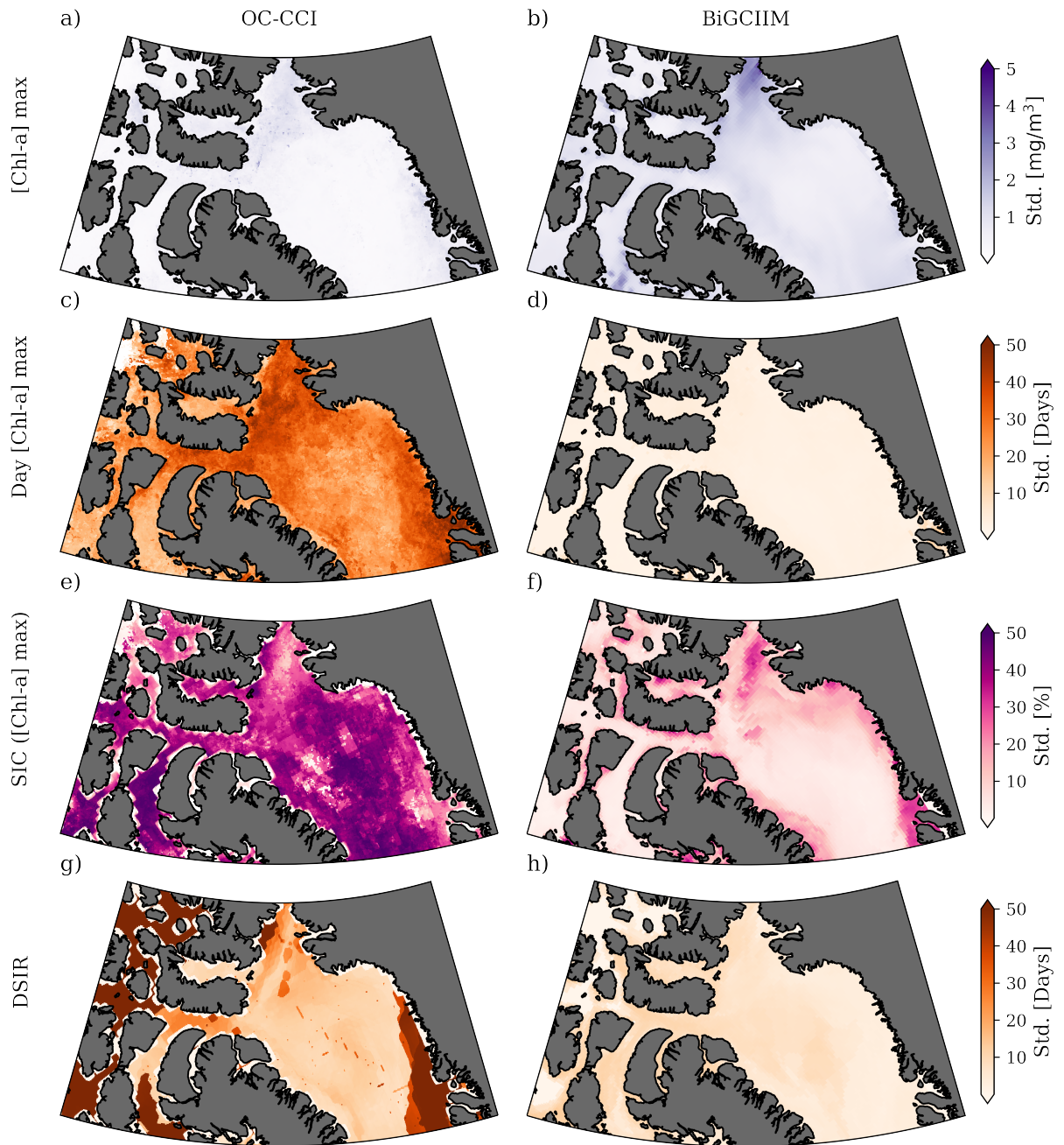


Figure 3.2: Standard deviation for average maximum (a,b) and Julian day (c,d) surface chlorophyll-a concentration, average sea ice concentration on day of maximum chlorophyll-a concentration (e, f) and average Julian day transition between ice covered area and open water (SIC = 15%) (g,h). From May 1st to September 30th for OC-CCI climatology (2002-2022) (a, c and g), sea ice concentration CDR climatology (2002-2022) (e) and BiGCIIM climatology (2002-2021) (b, d, f and h).

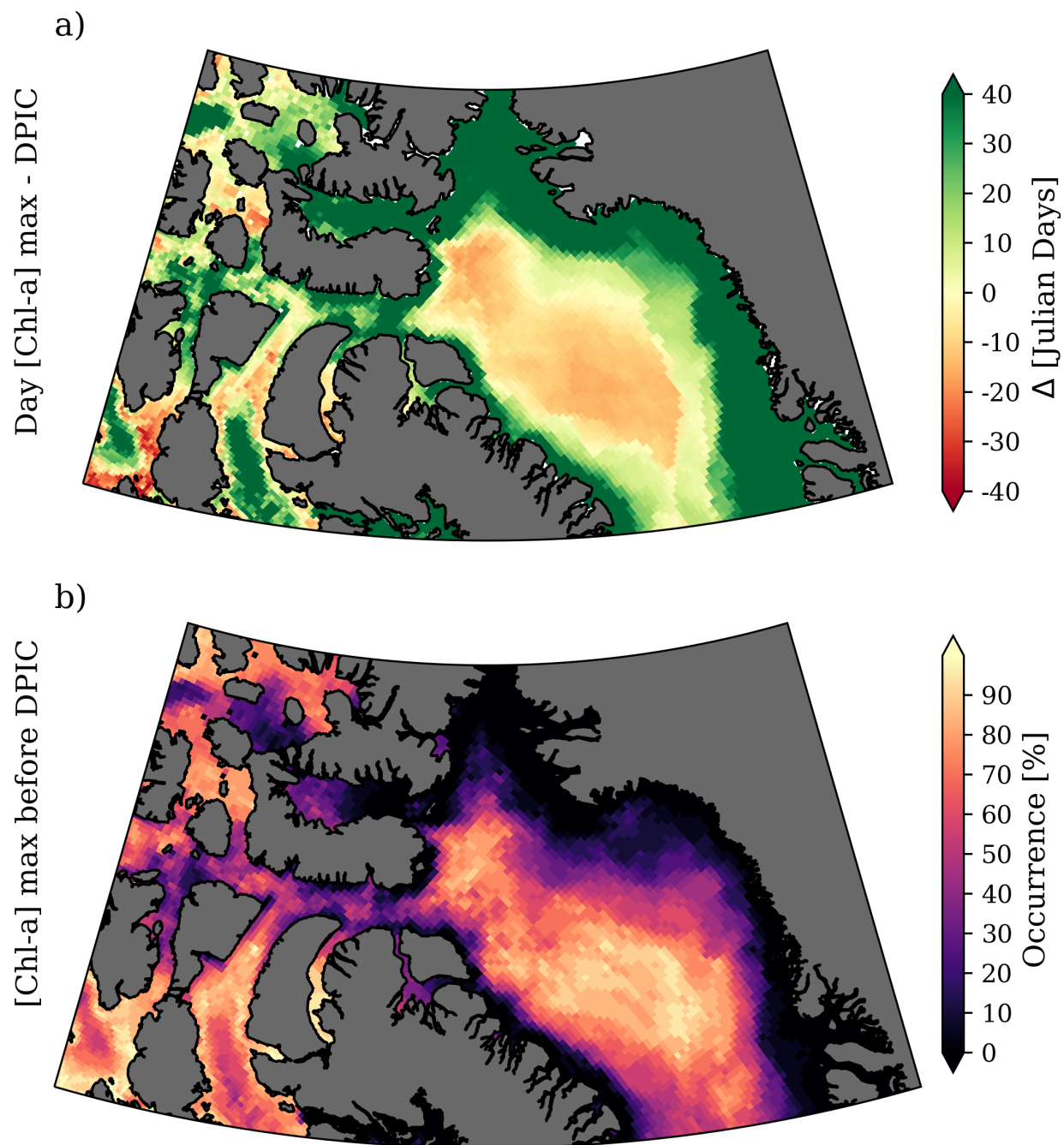


Figure 3.3: Difference between the average day of chlorophyll-a maximum and the day of partial ice cover (DPIC, i.e., the first Julian Day of $SIC \leq 85\%$) in BiGCIIM (a), and the climatological occurrence (%) when the average chlorophyll-a maximum occurs before the start of partial ice cover from 2002 to 2021 (b).

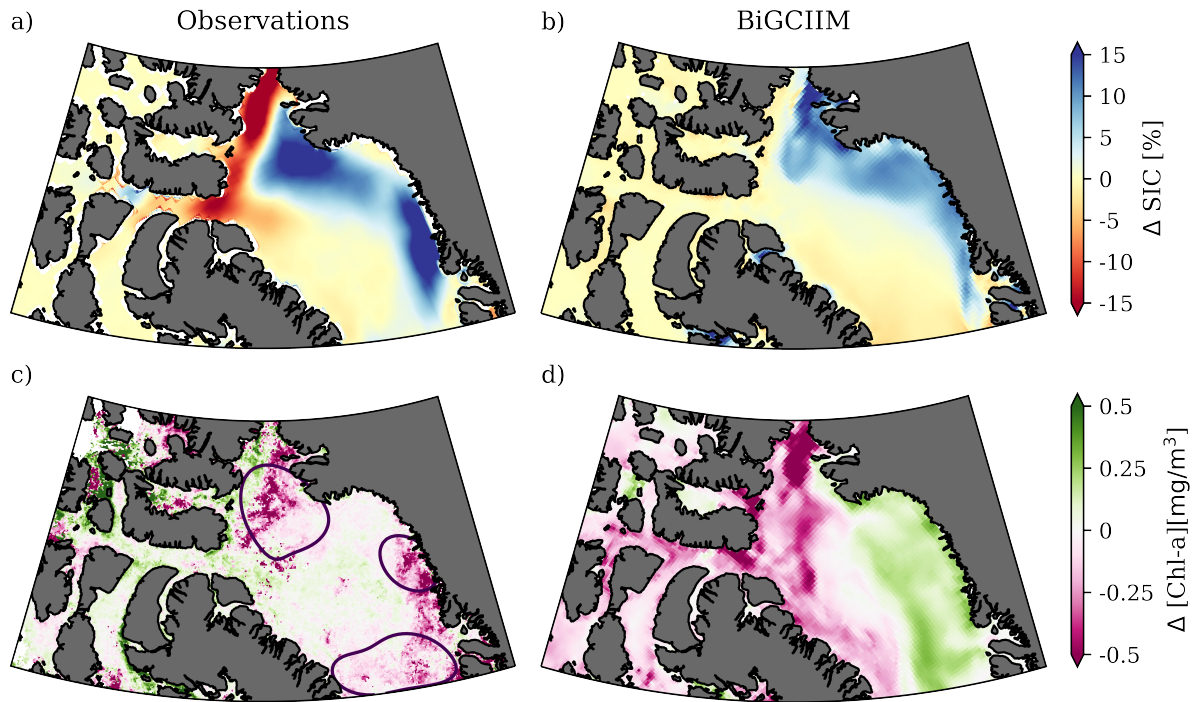


Figure 3.4: Difference in sea ice concentration in May (top panel) and chlorophyll-a concentrations from May 1st to September 30th (bottom panel) between the years with and without (2007, 2009, 2010, 2017, 2019) the Nares Strait Arch, for the observations from 2002 to 2022 (left column) and BiGCIIM from 2002 to 2021 (right column). Black contours indicate regions with a high grid density of data significant at the 95% level, smoothed using kernel density estimation (left column).

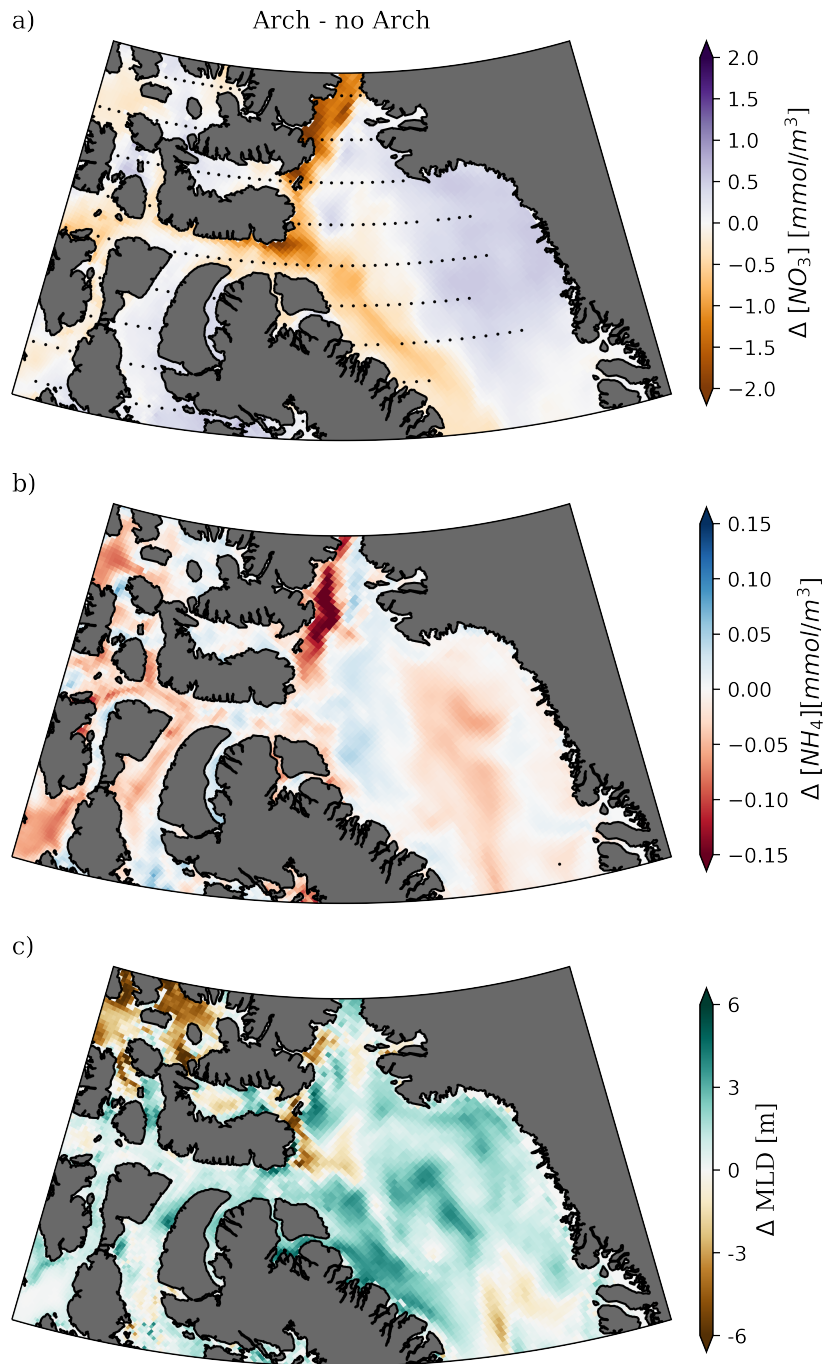


Figure 3.5: Difference in nitrate concentrations (a), ammonium concentrations (b) and mixed layer depth (c) from BiGCIIM between years with and without (2007, 2009, 2010, 2017, 2019, 2022) the Nares Strait Arch (NSA) from May 1st to September 30th for the period from 2002 to 2021. Black dots show grid cell with 95% significant difference.

Nares Strait arch – no arch slp composites
MERRA2 MAM 2002–2022

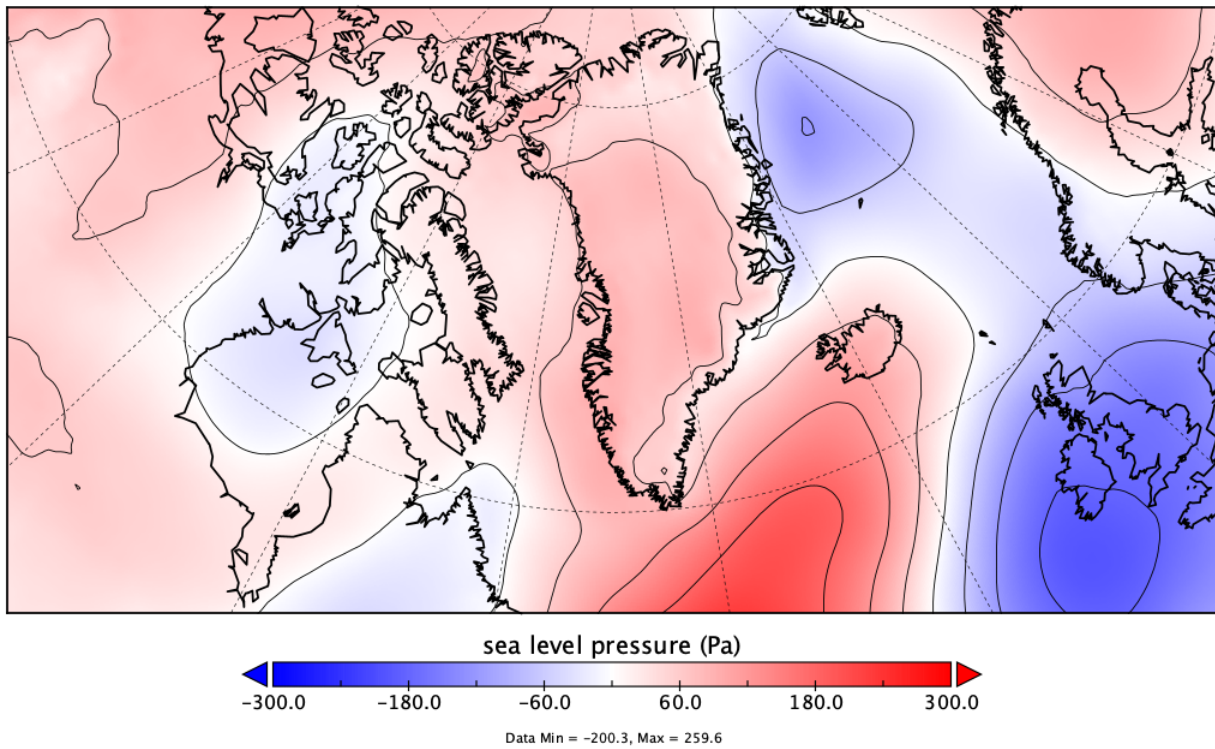


Figure 3.6: Difference in the composite of sea level pressure (Pa) from MERRA-2 between years with and without (2007, 2009, 2010, 2017, 2019, 2022) the Nares Strait Arch (NSA) for the month of March, April and May from 2002 to 2022.

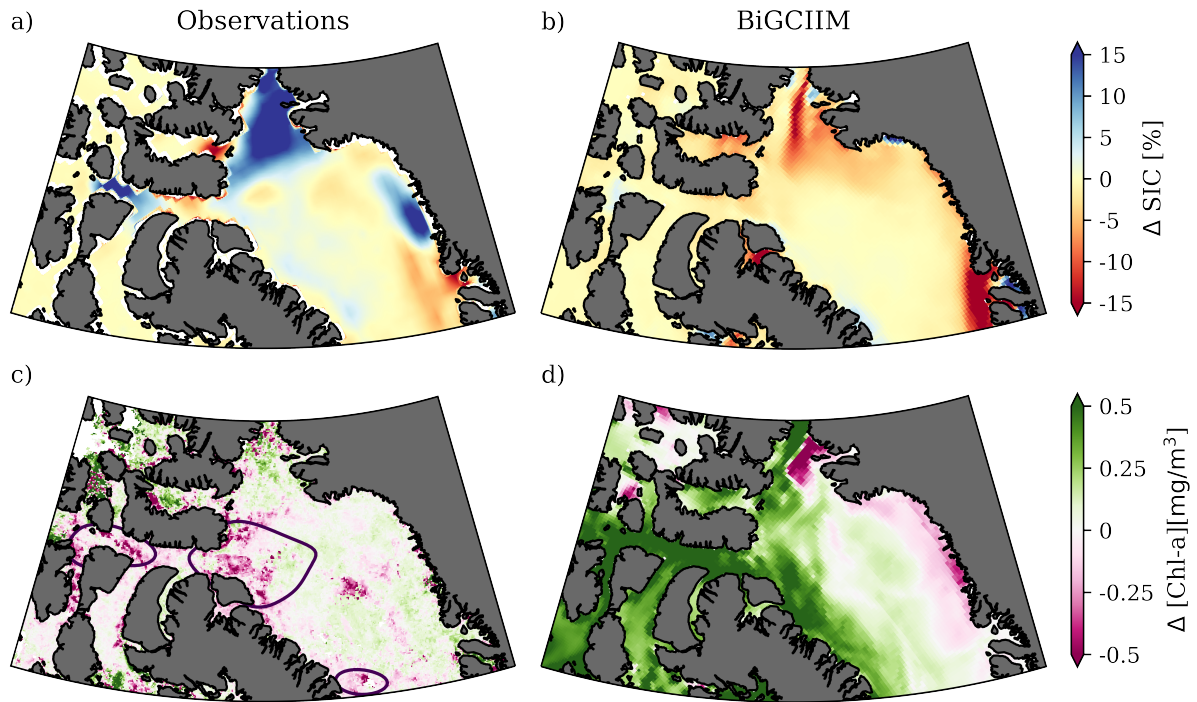


Figure 3.7: Difference in sea ice concentration in May (top panel) and chlorophyll-a concentrations from June 1st to September 30th (bottom panel) between the years with and without (2003, 2004, 2006, 2009, 2022) the Jones Sound Arches (JSA), for the observations from 2002 to 2022 (left column) and BiGCIIM from 2002 to 2021 (right column). Black contours indicate regions with a high grid density of data significant at the 95% level, smoothed using kernel density estimation (left column).

Jones Sound arch – no arch slp composites
MERRA2 MAM 2002–2022

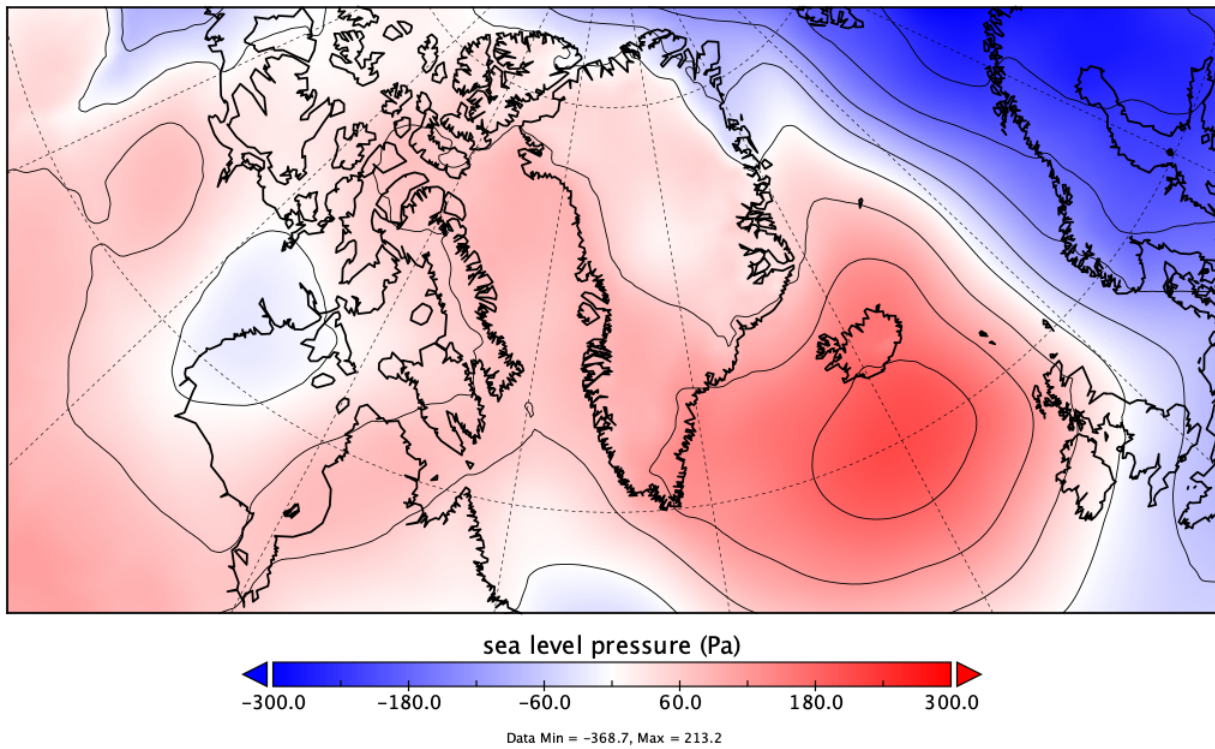


Figure 3.8: Difference in composite of sea level pressure (Pa) from MERRA-2 between years with and without (2003, 2004, 2006, 2009, 2022) the Jones Sound Arch (JSA) for the months of March, April and May from 2002 to 2022.

Chapter 4

Conclusions

The primary productivity in the Tallurutiup Imanga region is crucial for nearby communities but remains poorly understood. Light and nutrients limit biomass productivity, making its relationship to sea ice important for determining significant productive areas and times. This study examined the temporal and spatial patterns of maximum chlorophyll-a concentration and sea ice, the impact of open water formation in polynyas downstream of sea ice arches in Nares Strait and Jones Sound, and evaluated the BioGeo-Chemical Ice Incorporated model (BiGCIIM) in the region.

Results show that the timing and intensity of maximum chlorophyll-a concentrations ([chl-a]) are higher in Baffin Bay along the west Greenland coast and in the North Water, correlating with sea ice retreat. However, the model detected biomass maxima well before complete ice retreat, with as much as 90% sea ice cover in central Baffin Bay, indicating that satellite observations alone may be missing a significant contribution (i.e., under-ice bloom) to the total productivity, as suggested by many authors (3; 5; 54). Despite a 20% difference in biomass concentrations, both observations and the model agree that the NOW is the most productive region in Baffin Bay with the highest inter-annual variability, and with productivity limited by light. The model appears to have a negative thickness bias (thinner than observations); this combined with the simple two-ice cate-

gory model (ice and no ice) results in a pack ice that disappears up to three months before observations, particularly in Jones Sound and the Gulf of Boothia. This limitation prevents the use of the model to study mechanisms controlling phytoplankton productivity in these local regions with a lower resolution model.

To disentangle the light versus nutrient limitation on concentrations, results from a composite of years with and without sea ice arches in the Nares Strait (NSA) and Jones Sound (JSA) and their downstream polynyas are also analyzed. When the NSA is present, high SIC is observed in eastern NOW and less on the western side. Although the model cannot reproduce sea ice arches, its spatial pattern is similar to observations. This similarity is due to atmospheric wind anomalies associated with the North Atlantic Oscillation, where stronger northerly winds prevent arch formation in Nares Strait but promote them in Jones Sound, resulting in stronger simulated Baffin Island and West Greenland currents, and lower chlorophyll-a concentrations. In contrast, observations show higher biomass in the west and lower in the east, indicating that arch presence enhances mixing and nutrient import, increasing primary productivity downstream of the NSA.

The signal in sea ice concentration and [chl-a] associated with the presence or absence of an ice arch in Jones Sound (JSA) is not as easily interpreted, as sea ice concentration anomalies are opposite between observations and the model, with the key exception of lower SIC west of Coburg Island when the JSA forms. This and the fact that the model cannot simulate landfast ice prevent a meaningful interpretation of the results regarding the effect of sea ice arches in Jones Sound on primary productivity. Regardless, observations also do not show a coherent signal between SIC and [chl-a] with the presence or absence of the JSA, suggesting that light is not the main limiting factor, but rather the import of nutrients, presumably through glacier melt.

Further work should include running the coupled biogeochemical ice-ocean model with multiple ice thickness categories (e.g., LIM3), landfast sea ice parameterizations, and ice strength parameters that allow for sea ice arches to form; and including output diagnostics for both under-ice and open ocean productivity in order to compare with satellite observations that can only see ocean color in low sea ice concentration areas.

Chapter 5

Data Availability Statement

BioGeoChemical Ice Incorporated Model (BiGCIIM) outputs are available upon request at <https://borealisdata.ca/dataset.xhtml?persistentId=doi:10.5683/SP3/RE27IC>. Ocean Colour Climate Change Initiative dataset, Version 6.0, European Space Agency, available online at <http://www.esa-oceancolour-cci.org/>. NOAA/NSIDC Climate Data Record of Passive Microwave Sea ice Concentration datasets are available at <https://nsidc.org/data/g02202/versions/4> (?) To access sea ice arches data, please reach out to Dany Dumont via dany_dumont@uqar.ca

Appendix A

Appendices

1 Appendix A

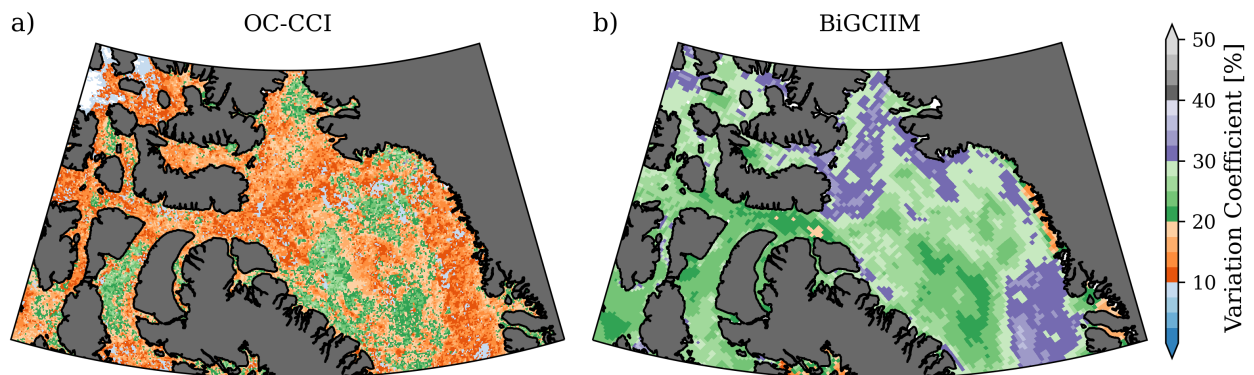


Figure A1: Average maximum chlorophyll-a concentrations variation coefficient (%) for the productive season, from May 1st to September 30th, for OC-CCI observations from 2002 to 2022 (a) and BiGCIIM from 2002 to 2021 (b).

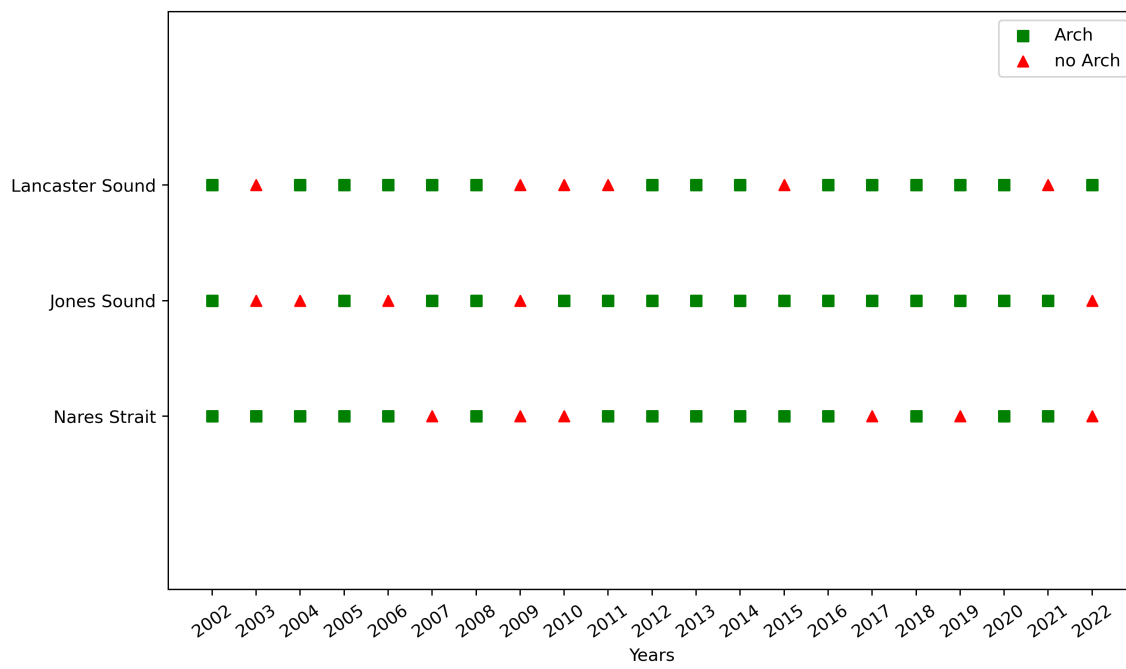


Figure A2: Temporal series of years with (green square) and without (red triangle) sea ice arch in the Nares Strait, Jones Sound and Lancaster Sound for May from 2002 to 2022.

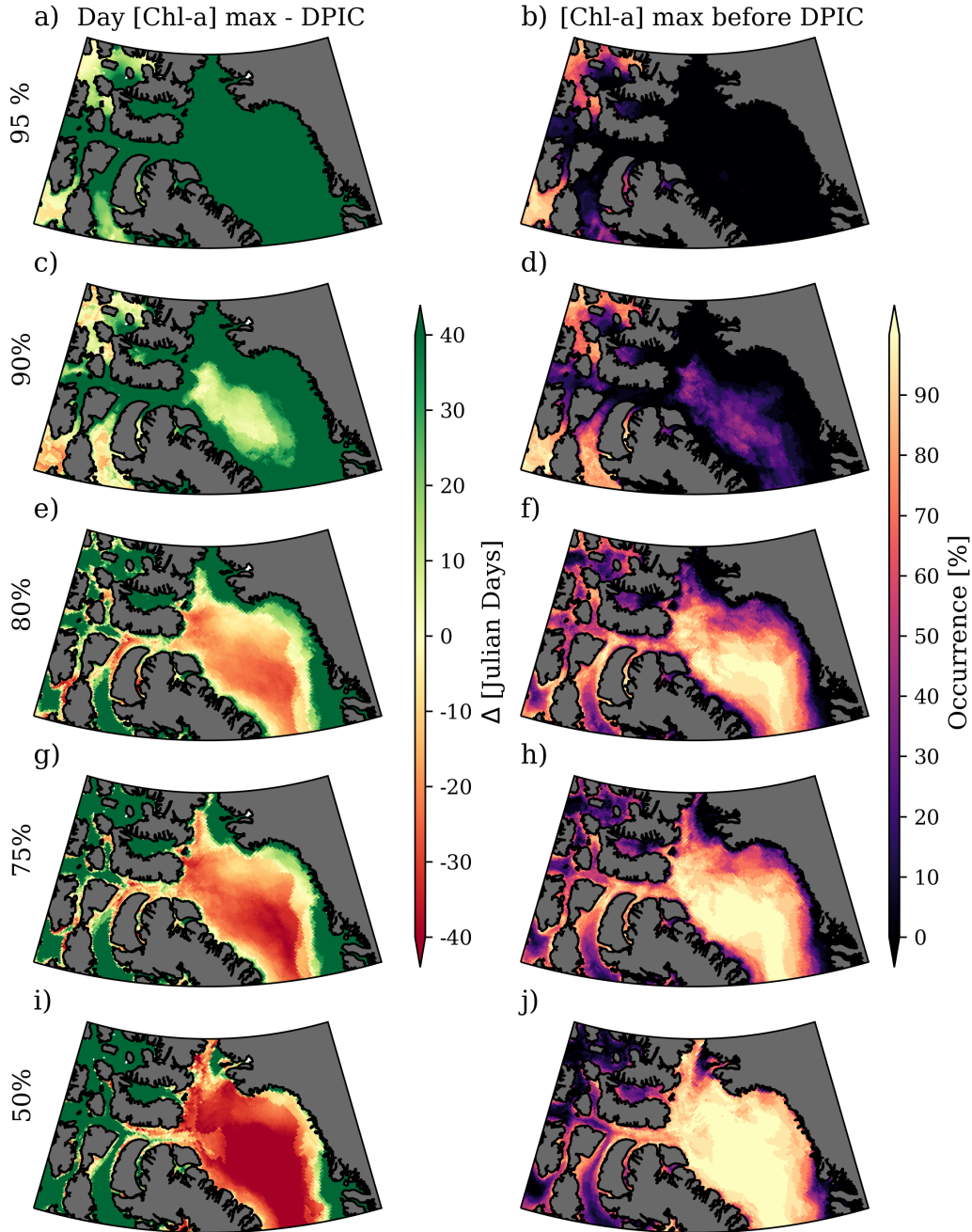


Figure A3: Difference between the average day of chlorophyll-a maximum and the day of partial ice cover (DPIC, i.e., the first Julian Day when SIC specified thresholds) in BiGCIIM (left column), and the occurrence (%) when the average chlorophyll-a maximum occurs before partial ice cover at different SIC thresholds (50%, 75%, 80%, 90%, and 95%) from 2002 to 2021 (right column).

Bibliography

- [1] ARDYNA, M., AND ARRIGO, K. R. Phytoplankton dynamics in a changing Arctic Ocean. *Nature Climate Change* 10, 10 (2020), 892–903.
- [2] ARDYNA, M., BABIN, M., GOSSELIN, M., DEVRED, E., RAINVILLE, L., AND TREMBLAY, J. É. Recent Arctic Ocean sea ice loss triggers novel fall phytoplankton blooms. *Geophysical Research Letters* 41, 17 (2014), 6207–6212.
- [3] ARDYNA, M., MUNDY, C., MAYOT, N., MATTHES, L. C., OZIEL, L., HORVAT, C., LEU, E., ASSMY, P., HILL, V., MATRAI, P. A., ET AL. Under-ice phytoplankton blooms: Shedding light on the “invisible” part of arctic primary production. *Frontiers in Marine Science* 7 (2020), 608032.
- [4] ARRIGO, K. R., VAN DIJKEN, G., AND PABI, S. Impact of a shrinking Arctic ice cover on marine primary production. *Geophysical Research Letters* 35, 19 (oct 2008), 1–6.
- [5] ARRIGO, K. R., VAN DIJKEN, G., AND PABI, S. Impact of a shrinking arctic ice cover on marine primary production. *Geophysical Research Letters* 35, 19 (2008).
- [6] ARRIGO, K. R., AND VAN DIJKEN, G. L. Continued increases in arctic ocean primary production. *Progress in Oceanography* 136 (2015), 60–70. Synthesis of Arctic Research (SOAR).
- [7] BABIN, M., BÉLANGER, S., ELLINGSEN, I., FOREST, A., LE FOUEST, V., LACOUR, T., ARDYNA, M., AND SLAGSTAD, D. Estimation of primary production in the arctic ocean using ocean colour remote sensing and coupled physical–biological models:

- Strengths, limitations and how they compare. *Progress in Oceanography* 139 (2015), 197–220. Overarching perspectives of contemporary and future ecosystems in the Arctic Ocean.
- [8] BARBEDO, L., BÉLANGER, S., AND TREMBLAY, J. É. Climate control of sea-ice edge phytoplankton blooms in the Hudson Bay system. *Elementa* 8, 1 (dec 2020).
- [9] BÉLANGER, S., BABIN, M., AND TREMBLAY, J.-É. Increasing cloudiness in Arctic dampens the increase in phytoplankton primary production due to sea ice receding. *Biogeosciences* 10, 6 (jun 2013), 4087–4101.
- [10] BERGERON, M., AND TREMBLAY, J.-É. Shifts in biological productivity inferred from nutrient drawdown in the southern beaufort sea (2003–2011) and northern baffin bay (1997–2011), canadian arctic. *Geophysical Research Letters* 41, 11 (2014), 3979–3987.
- [11] BHATIA, M. P., WATERMAN, S., BURGESS, D. O., WILLIAMS, P. L., BUNDY, R. M., MELLETT, T., ROBERTS, M., AND BERTRAND, E. M. Glaciers and Nutrients in the Canadian Arctic Archipelago Marine System. *Global Biogeochemical Cycles* 35, 8 (2021), 1–24.
- [12] BLAIS, M., ARDYNA, M., GOSSELIN, M., DUMONT, D., BÉLANGER, S., TREMBLAY, J.-É., GRATTON, Y., MARCHESE, C., AND POULIN, M. Contrasting interannual changes in phytoplankton productivity and community structure in the coastal Canadian Arctic Ocean. *Limnology and Oceanography* 62, 6 (nov 2017), 2480–2497.
- [13] CAPPELEN, J., VINTHER, B., KERN-HANSEN, C., VAARBY, E., AND VISKUM, P. *Greenland: DMI historical climate data collection 1784-2017*. Danish Meteorological Institute Copenhagen, Denmark, 2018.
- [14] CASTRO DE LA GUARDIA, L., GARCIA-QUINTANA, Y., CLARET, M., HU, X., GALBRAITH, E., AND MYERS, P. G. Assessing the role of high-frequency winds and sea ice loss on arctic phytoplankton blooms in an ice-ocean-biogeochemical model. *Journal of Geophysical Research: Biogeosciences* 124, 9 (2019), 2728–2750.

- [15] CAVALIERI, D. J., GLOERSEN, P., AND CAMPBELL, W. J. Determination of sea ice parameters with the nimbus 7 smmr. *Journal of Geophysical Research: Atmospheres* 89, D4 (1984), 5355–5369.
- [16] COMISO, J. C. Characteristics of arctic winter sea ice from satellite multispectral microwave observations. *Journal of Geophysical Research: Oceans* 91, C1 (1986), 975–994.
- [17] DESCHEPPER, I. *The biogeochemical dynamics of Canada's largest inland Arctic sea, the Hudson Bay Complex, revealed through the use of numerical models*. Phd thesis, Université Laval, Quebec, QC, Canada, June 2024.
- [18] DESCHEPPER, I., MYERS, P. G., LAVOIE, D., PAPAKYRIAKOU, T., AND MAPS, F. Understanding the physical forcings behind the biogeochemical productivity of the hudson bay complex. *Journal of Geophysical Research: Biogeosciences* 128, 6 (2023), e2022JG007294.
- [19] DOUGLAS, C. C., BRIGGS, N., BROWN, P., MACGILCHRIST, G., AND NAVEIRA GARABATO, A. Exploring the relationship between sea ice and phytoplankton growth in the weddell gyre using satellite and argo float data. *Ocean Science* 20, 2 (2024), 475–497.
- [20] DUMONT, D., GRATTON, Y., AND ARBETTER, T. E. Modeling the dynamics of the north water polynya ice bridge. *Journal of Physical Oceanography* 39, 6 (2009), 1448–1461.
- [21] EICKEN, H., GRENFELL, T., PEROVICH, D., RICHTER-MENGE, J., AND FREY, K. Hydraulic controls of summer arctic pack ice albedo. *Journal of Geophysical Research: Oceans* 109, C8 (2004).
- [22] GELARO, R., MCCARTY, W., SUÁREZ, M. J., TODLING, R., MOLOD, A., REICHLER, K. W., COY, L., CULLATHER, R., DRAPER, C., AKELLA, S., ET AL. The modern-era retrospective analysis for research and applications, 2017.

- [23] GLISSENAAR, I. A., LANDY, J. C., BABB, D. G., DAWSON, G. J., AND HOWELL, S. E. L. A long-term proxy for sea ice thickness in the canadian arctic: 1996–2020. *The Cryosphere* 17, 8 (2023), 3269–3289.
- [24] GLOBAL MODELING AND ASSIMILATION OFFICE, AND PAWSON, S. MERRA-2 tavgM_2d_slv_Nx: 2d,monthly mean,Time-Averaged,Single-Level,Assimilation,Single-Level diagnostics v5.12.4, 2015.
- [25] HOWELL, S., BABB, D., LANDY, J. C., MOORE, G., MONTPETIT, B., AND BRADY, M. A comparison of arctic ocean sea ice export between nares strait and the canadian arctic archipelago. *Journal of Geophysical Research: Oceans* 128, 4 (2023), e2023JC019687.
- [26] HU, X., SUN, J., CHAN, T. O., AND MYERS, P. G. Thermodynamic and dynamic ice thickness contributions in the canadian arctic archipelago in nemo-lim2 numerical simulations. *The Cryosphere* 12, 4 (2018), 1233–1247.
- [27] HU, X., SUN, J., CHAN, T. O., AND MYERS, P. G. Thermodynamic and dynamic ice thickness contributions in the canadian arctic archipelago in nemo-lim2 numerical simulations. *The Cryosphere* 12, 4 (2018), 1233–1247.
- [28] HUOT, Y., BABIN, M., BRUYANT, F., GROB, C., TWARDOWSKI, M., AND CLAUSTRÉ, H. Relationship between photosynthetic parameters and different proxies of phytoplankton biomass in the subtropical ocean. *Biogeosciences* 4, 5 (2007), 853–868.
- [29] HURRELL, J. W., AND DESER, C. North atlantic climate variability: The role of the north atlantic oscillation. *Journal of Marine Systems* 79, 3 (2010), 231–244. Impact of climate variability on marine ecosystems: A comparative approach.
- [30] IOCCG. *Ocean Colour Remote Sensing in Polar Seas Report of an IOCCG working group on Ocean Colour Remote Sensing in Polar Seas, chaired and based on contributions from (in alphabetical order)*. No. 16. Dartmouth, Canada, 2015.

- [31] KERN, S., LAVERGNE, T., PEDERSEN, L. T., TONBOE, R. T., BELL, L., MEYER, M., AND ZEIGERMANN, L. Satellite passive microwave sea-ice concentration data set intercomparison using landsat data. *The Cryosphere* 16, 1 (2022), 349–378.
- [32] KIMMTRITZ, M., LOSCH, M., AND DANILOV, S. A comparison of viscous-plastic sea ice solvers with and without replacement pressure. *Ocean Modelling* 115 (2017), 59–69.
- [33] KLEIN, B., LEBLANC, B., MEI, Z. P., BERET, R., MICHAUD, J., MUNDY, C. J., VON QUILLFELDT, C. H., GARNEAU, M. E., ROY, S., GRATTON, Y., COCHRAN, J. K., BELANGER, S., LAROUCHE, P., PAKULSKI, J. D., RIVKIN, R. B., AND LEGENDRE, L. Phytoplankton biomass, production and potential export in the North Water. *Deep-Sea Research* 49, 22-23 (2002), 4983–5002.
- [34] KWIATKOWSKA, E. Comparisons of daily global ocean color data sets: Modis-terra/aqua and seawifs. *MODIS Validation, Data Merger and Other Activities Accomplished by the SIMBIOS Project: 2002-2003* (2003), 2.
- [35] KWOK, R. Arctic sea ice thickness, volume, and multiyear ice coverage: losses and coupled variability (1958–2018). *Environmental Research Letters* 13, 10 (2018), 105005.
- [36] KYHN, L. A., AND MOSBECH, A. White paper-north water polynya conference. In *North Water Polynya Conference* (2019), Aarhus Universitet.
- [37] L.A. MYSAK, R.G. INGRAM, J. W., AND VAN DER BAAREN, A. The anomalous sea-ice extent in hudson bay, baffin bay and the labrador sea during three simultaneous nao and enso episodes. *Atmosphere-Ocean* 34, 2 (1996), 313–343.
- [38] LE FOUEST, V., BABIN, M., AND TREMBLAY, J.-E. The fate of riverine nutrients on arctic shelves. *Biogeosciences* 10, 6 (2013), 3661–3677.

- [39] LEWIS, K. M., VAN DIJKEN, G. L., AND ARRIGO, K. R. Changes in phytoplankton concentration now drive increased Arctic Ocean primary production. *Science* 369, 6500 (2020), 198–202.
- [40] LI, W. K. W., MCLAUGHLIN, F. A., LOVEJOY, C., AND CARMACK, E. C. Smallest algae thrive as the Arctic Ocean freshens. *Science* 326, 5952 (oct 2009), 539.
- [41] LONG, M. C., LINDSAY, K., AND HOLLAND, M. M. Modeling photosynthesis in sea ice-covered waters. *Journal of Advances in Modeling Earth Systems* 7, 3 (sep 2015), 1189–1206.
- [42] MADEC, G., BELL, M., BLAKER, A., BRICAUD, C., BRUCIAFERRI, D., CASTRILLO, M., CALVERT, D., CHANUT, J., CLEMENTI, E., COWARD, A., EPICOCO, I., ÉTHÉ, C., GANDERTON, J., HARLE, J., HUTCHINSON, K., IOVINO, D., LEA, D., LOVATO, T., MARTIN, M., MARTIN, N., MELE, F., MARTINS, D., MASSON, S., MATHIOT, P., MELE, F., MOCAVERO, S., MÜLLER, S., NURSER, A. G., PARONUZZI, S., PELTIER, M., PERSON, R., ROUSSET, C., RYNDERS, S., SAMSON, G., TÉCHENÉ, S., VANCOPPENOLLE, M., AND WILSON, C. Nemo ocean engine reference manual, July 2023.
- [43] MARCHESI, C., ALBOUY, C., TREMBLAY, J.-É., DUMONT, D., D’ORTENZIO, F., VISSAULT, S., AND BÉLANGER, S. Changes in phytoplankton bloom phenology over the north water (now) polynya: a response to changing environmental conditions. *Polar Biology* 40 (2017), 1721–1737.
- [44] MASSONNET, F., FICHEFET, T., GOOSSE, H., VANCOPPENOLLE, M., MATHIOT, P., AND KÖNIG BEATTY, C. On the influence of model physics on simulations of arctic and antarctic sea ice. *The Cryosphere* 5, 3 (2011), 687–699.
- [45] MEIER, W. N., FETTERER, F., WINDNAGEL, A. K., AND STEWART, S. NOAA/NSIDC Climate Data Record of Passive Microwave Sea Ice Concentration, Version 4. National Snow and Ice Data Center, 2021. 15-03-2024.

- [46] MEIER, W. N., STEWART, J. S., WINDNAGEL, A., AND FETTERER, F. M. Comparison of hemispheric and regional sea ice extent and area trends from noaa and nasa passive microwave-derived climate records. *Remote Sensing* 14, 3 (2022), 619.
- [47] MICHEL, C., HAMILTON, J., HANSEN, E., BARBER, D., REIGSTAD, M., IACOZZA, J., SEUTHE, L., AND NIEMI, A. Arctic ocean outflow shelves in the changing arctic: A review and perspectives. *Progress in Oceanography* 139 (2015), 66–88. Overarching perspectives of contemporary and future ecosystems in the Arctic Ocean.
- [48] MOORE, G., HOWELL, S., AND BRADY, M. Evolving relationship of nares strait ice arches on sea ice along the strait and the north water, the arctic’s most productive polynya. *Scientific Reports* 13, 1 (2023), 9809.
- [49] MUNDY, C. J., GOSSELIN, M., GRATTON, Y., BROWN, K., GALINDO, V., CAMPBELL, K., LEVASSEUR, M., BARBER, D., PAPAKYRIAKOU, T., AND BÉLANGER, S. Role of environmental factors on phytoplankton bloom initiation under landfast sea ice in Resolute Passage , Canada. *Mar. Ecol. Progr. Series* 497, 2009 (2014), 39–49.
- [50] MYERS, P. G., BARBER, D., BRAUN, M., BUCHART, L., DE LA GUARDIA, L. C., DESCHEPPER, I., DUPONT, F., EHN, J., GARCIA-QUINTANA, Y., GILLARD, L. C., ET AL. An overview of the nemo modelling for the baysys project. *Elementa Science of the Anthropocene* 12, 1 (2024), 00111.
- [51] NICOLAUS, M., KATLEIN, C., MASLANIK, J., AND HENDRICKS, S. Changes in arctic sea ice result in increasing light transmittance and absorption. *Geophysical Research Letters* 39, 24 (2012).
- [52] OF THE ENVIRONMENT, M., CLIMATE CHANGE FOR THE PURPOSES OF THE PARKS CANADA AGENCY, M. O. F., OCEANS, AND CANADIAN COAST GUARD, MINISTER OF TRANSPORT, Q. I. A. Tallurutiup imanga national marine conservation area, August 2019.

- [53] OLIVIER, F., GAILLARD, B., MEZIANE, T., TREMBLAY, R., BÉLANGER, S., GOSSELIN, M., CHAUVAUD, L., MARTEL, A. L., RYSGAARD, S., OLIVIER, A.-H., MARS, J., GERBER, S., AND ARCHAMBAULT, P. Shells of the bivalve *Astarte moerchi* give new evidence of a strong pelagic-benthic coupling shift occurring since the late 1970s in the North Water polynya. *Phil.Trans.R.Soc.A* 378 (2020), 20190353.
- [54] OZIEL, L., MASSICOTTE, P., RANDELHOFF, A., FERLAND, J., VLADOIU, A., LA-COUR, L., GALINDO, V., LAMBERT-GIRARD, S., DUMONT, D., CUYPERS, Y., ET AL. Environmental factors influencing the seasonal dynamics of spring algal blooms in and beneath sea ice in western baffin bay. *Elem Sci Anth* 7 (2019), 34.
- [55] PARKS CANADA AGENCY, AND GOVERNMENT OF CANADA. Why protect tallurutiup imanga? <https://parks.canada.ca/amnc-nmca/cnamnc-cnmca/tallurutiup-imanga/proteger-protect>, July 2019. Accessed: 2024-4-8.
- [56] POLASHENSKI, C., PEROVICH, D., AND COURVILLE, Z. The mechanisms of sea ice melt pond formation and evolution. *Journal of Geophysical Research: Oceans* 117, C1 (2012).
- [57] RAJULAPATI, C. R., PAPALEXIOU, S. M., CLARK, M. P., AND POMEROY, J. W. The perils of regridding: examples using a global precipitation dataset. *Journal of Applied Meteorology and Climatology* 60, 11 (2021), 1561–1573.
- [58] RIBEIRO, S., LIMOGES, A., MASSÉ, G., JOHANSEN, K. L., COLGAN, W., WECKSTRÖM, K., JACKSON, R., GEORGIADIS, E., MIKKELSEN, N., KUIJPERS, A., ET AL. Vulnerability of the north water ecosystem to climate change. *Nature Communications* 12, 1 (2021), 4475.
- [59] RIENECKER, M. M., SUAREZ, M. J., GELARO, R., TODLING, R., BACMEISTER, J., LIU, E., BOSILOVICH, M. G., SCHUBERT, S. D., TAKACS, L., KIM, G.-K., ET AL. Merra: Nasa’s modern-era retrospective analysis for research and applications. *Journal of climate* 24, 14 (2011), 3624–3648.

- [60] SATHYENDRANATH, S., BREWIN, R. J., BROCKMANN, C., BROTHAS, V., CALTON, B., CHUPRIN, A., CIPOLASLINI, P., COUTO, A. B., DINGLE, J., DOERFFER, R., ET AL. An ocean-colour time series for use in climate studies: the experience of the ocean-colour climate change initiative (oc-cci). *Sensors* 19, 19 (2019), 4285.
- [61] SATHYENDRANATH, S., BREWIN, R. J., BROCKMANN, C., BROTHAS, V., CALTON, B., CHUPRIN, A., CIPOLLINI, P., COUTO, A. B., DINGLE, J., DOERFFER, R., DONLON, C., DOWELL, M., FARMAN, A., GRANT, M., GROOM, S., HORSEMAN, A., JACKSON, T., KRASEMANN, H., LAVENDER, S., MARTINEZ-VICENTE, V., MAZERAN, C., MÉLIN, F., MOORE, T. S., MÜLLER, D., REGNER, P., ROY, S., STEELE, C. J., STEINMETZ, F., SWINTON, J., TABERNER, M., THOMPSON, A., VALENTE, A., ZÜHLKE, M., BRANDO, V. E., FENG, H., FELDMAN, G., FRANZ, B. A., FROUIN, R., GOULD, R. W., HOOKER, S. B., KAHRU, M., KRATZER, S., MITCHELL, B. G., MULLER-KARGER, F. E., SOSIK, H. M., VOSS, K. J., WERDELL, J., AND PLATT, T. An ocean-colour time series for use in climate studies: The experience of the ocean-colour climate change initiative (oc-cci). *Sensors* 19, 19 (2019).
- [62] SATHYENDRANATH, S., JACKSON, T., BROCKMANN, C., BROTHAS, V., CALTON, B., CHUPRIN, A., CLEMENTS, O., CIPOLLINI, P., DANNE, O., DINGLE, J., DONLON, C., GRANT, M., GROOM, S., KRASEMANN, H., LAVENDER, S., MAZERAN, C., MÉLIN, F., MÜLLER, D., STEINMETZ, F., VALENTE, A., ZÜHLKE, M., FELDMAN, G., FRANZ, B., FROUIN, R., WERDELL, J., AND PLATT, T. ESA Ocean Colour Climate Change Initiative (Ocean.Colour_cci): Version 5.0 Data. NERC EDS Centre for Environmental Data Analysis, 19 May 2021, 2021.
- [63] SCHULZWEIDA, U., KORNBLUEH, L., AND QUAST, R. Cdo user guide, 2019.
- [64] SERVICE, C. I. Canadian ice service arctic regional sea ice charts in sigrid-3 format, version 1, 2009.

- [65] SIBERT, V., ZAKARDJIAN, B., SAUCIER, F., GOSSELIN, M., STARR, M., AND SENNEVILLE, S. Spatial and temporal variability of ice algal production in a 3d ice–ocean model of the hudson bay, hudson strait and foxe basin system. *Polar Research* 29, 3 (2010), 353–378.
- [66] SONG, H., JI, R., JIN, M., LI, Y., FENG, Z., VARPE, Ø., AND DAVIS, C. S. Strong and regionally distinct links between ice-retreat timing and phytoplankton production in the arctic ocean. *Limnology and Oceanography* 66, 6 (2021), 2498–2508.
- [67] STAMMERJOHN, S., MASSOM, R., RIND, D., AND MARTINSON, D. Regions of rapid sea ice change: An inter-hemispheric seasonal comparison. *Geophysical Research Letters* 39, 6 (2012).
- [68] STERN, H. L., AND HEIDE-JØRGENSEN, M. P. Trends and variability of sea ice in baffin bay and davis strait, 1953–2001. *Polar Research* 22, 1 (2003), 11–18.
- [69] TOULLEC, J., MORICEAU, B., VINCENT, D., GUIDI, L., LAFOND, A., AND BABIN, M. Processes controlling aggregate formation and distribution during the arctic phytoplankton spring bloom in baffin bay. *Elem Sci Anth* 9, 1 (2021), 00001.
- [70] TREMBLAY, J.-É., AND GAGNON, J. The effects of irradiance and nutrient supply on the productivity of arctic waters: a perspective on climate change. In *Influence of climate change on the changing arctic and sub-arctic conditions*. Springer, 2009, pp. 73–93.
- [71] TREMBLAY, J.-É., GRATTON, Y., CARMACK, E. C., PAYNE, C. D., AND PRICE, N. M. Impact of the large-scale arctic circulation and the north water polynya on nutrient inventories in baffin bay. *Journal of Geophysical Research: Oceans* 107, C8 (2002), 26–1.
- [72] TREMBLAY, J.-É., HATTORI, H., MICHEL, C., RINGUETTE, M., MEI, Z.-P., LOVEJOY, C., FORTIER, L., HOBSON, K. A., AMIEL, D., AND COCHRAN, J. K. Trophic structure and pathways of biogenic carbon flow in the eastern North Water Polynya. *Progress in Oceanography* 71 (2006), 402–425.

- [73] TREMBLAY, J.-É., ROBERT, D., VARELA, D. E., LOVEJOY, C., DARNIS, G., NELSON, R. J., AND SASTRI, A. R. Current state and trends in canadian arctic marine ecosystems: I. primary production. *Climatic Change* 115 (2012), 161–178.
- [74] VANCOPPENOLLE, M., BOUILLON, S., FICHEFET, T., GOOSSE, H., LECOMTE, O., MORALES MAQUEDA, M., AND MADEC, G. The louvain-la-neuve sea ice model. *Notes du pole de modélisation, Institut Pierre-Simon Laplace (IPSL), Paris, France* 31 (2012).
- [75] VINCENT, R. A study of the north water polynya ice arch using four decades of satellite data. *Scientific Reports* 9, 1 (2019), 20278.
- [76] VINCENT, R. F. An assessment of the lancaster sound polynya using satellite data 1979 to 2022. *Remote Sensing* 15, 4 (2023), 954.
- [77] WANG, X., LIU, Y., KEY, J. R., AND DWORAK, R. A new perspective on four decades of changes in arctic sea ice from satellite observations. *Remote Sensing* 14, 8 (2022).